What Drives the SASI in Core-Collapse Supernova?

John M. Blondin
Department of Physics, North Carolina State University. Raleigh, NC
john_blondin@ncsu.edu
and

Cody A. Melton
Department of Physics, North Carolina State University. Raleigh, NC
camelto2@ncsu.edu

ABSTRACT

A critical component behind a core-collapse supernova is the spherical accretion shock instability, or SASI. Two theories describing this mechanism have been proposed. The advective-acoustic mechanism says entropy perturbations generated at the shock travel radially inward with the accretion flow, which then couple to an acoustic wave that travels radially outward to the shock. Amplification at the inner coupling radius leads to amplification of this closed loop, driving the instability. The acoustic mechanism states that the SASI is purely an acoustic phenomenon in which a sound wave travels around the circumference of the shock. Amplification of this wave driven by continued perturbation of the accretion shock. We investigate these two theories by observing the SASI in a regime where the period of oscillation for each mechanism becomes disparate. Because the sound speed behind the shock is determined by the gravitational potential and the post shock flow speed is a strong function of the ratio of specific heats, γ, the advective-acoustic mechanism has a much longer timescale for small values of γ. By using two-dimensional hydrodynamic simulations, we show that the oscillation period of the SASI is between the acoustic and advective-acoustic prediction, suggesting that the SASI operates as a combination of both descriptions.

Subject headings: accretion, accretion disks - hydrodynamics - shock waves - supernovae: general - turbulence

1. INTRODUCTION

Core-collapse supernovae have been subject to immense research over the past few years. An interesting part of this research has focused on the post-bounce accretion phase prior to explosion where a stable accretion shock is formed. This shock does not stay stable for long, only about 300 ms (Mezzacappa et al. 2001). Once this becomes unstable, we have a linear phase of growth which leads into a nonlinear phase, ending the post-bounce phase of the supernovae.

Janka (2001) gives a clear analytic description of this post-bounce phase. During the post-bounce phase, outer core matter accretes down onto the shock approximately half the free-fall velocity. As this material passes the shock, the material decelerates and settles onto the proto-neutron star (PNS). This material consists mostly of electrons, positrons, and radiation that have an adiabatic index, γ, of 4/3. This spherical accretion shock is stable due to the continuous accretion of matter and the cooling of matter by neutrinos as is settles on the PNS. The research in this post-bounce phase has led to the discovery of the spherical accretion shock instability, or SASI. Blondin et al. (2003) showed that the accretion shock becomes dynamically unstable. Small entropy perturba-

tions lead to turbulence behind the shock causing the accretion shock to be spherically unstable. This instability is a linear process in which various modes are excited in the early time evolution. Given time, the SASI operates under the $l = 1$ mode in terms of Legendre polynomials, which dominates the linear growth and is always unstable (Blondin et al. 2006). This axisymmetric mode can be thought of as a linear combination of the non-axisymmetric mode m=1 traveling in opposite directions (Blondin et al. 2007). The l=1 mode has been shown to dominate the SASI in many 2D simulations. Ohnishi (2006) used varied neutrino luminosity to compare stable and unstable neutrino-driven convection, all showing that the l=1 mode dominates the process. Foglizzo et al. (2007) reaffirms that the l=1 "sloshing" mode is dominant but with a different conclusion.

Blondin et al. (2006) describes the SASI as an acoustic phenomenon in which acoustic waves travel within the boundaries of the SAS. Due to the l=1 mode, the acoustic mecanism can be described as a pressure wave that travels around the interior circumference of the shock, r_a, and "sloshes" back and forth between the poles (For a visual of this, see Figure 7 from Blondin et al 2006). If there is amplification of this wave, it will interact with the shock such that it enters the non-linear phase of growth which leads to the supernova explosion. An alternate description of the SASI has been proposed by Foglizzo et al. (2007). The advective-acoustic description of the SASI says pressure perturbations generated at the SAS fall radially inward toward the PNS. These perturbations then couple at a critical radius, r_c, larger than the radius of the PNS to pressure waves, which travel outward back to the shock. If this wave amplifies and interacts with the SAS, it creates the instability known as the SASI. The wave grows linearly in the l=1 mode and then enters the non-linear phase to create the explosion.

These descriptions are inconsistent with one another and must be described in order to fully understand supernova. Previous research has shown that both the acoustic and advective-acoustic cycle oscillate at approximately the same period for γ=4/3, thus making it very difficult to distinguish between the two descriptions. In order to distinguish between the two models, an analytic model will be used to observe a regime where the oscillation period for each mechanism becomes disparate. Then using 2D simulations, we will use the total linear momentum to track the amplitude of the SASI, where we can then extract an oscillation frequency for the SASI. Comparing this oscillation frequency to our analytic model will provide evidence that the SASI does not favor either model. To fully describe the SASI, come combination of both will be needed.

In this paper, we will investigate the SASI and the mechanisms describing it by using an approach that is independent and unbiased to both mechanisms, in order to determine if the SASI favors either model. In §2, we describe the numerical model, both radiative and adiabatic, that will distinguish between the acoustic and advective-acoustic mechanism. In §3, we present the results of our one dimension analysis to check for radial stability. In §4, we analyze the adiabatic two-dimensional hydrodynamic simulations of the the SASI. In § 5, we analyze the radiative simulations of the SASI In §6, we analyze the advective-acoustic mechanism against our results. In §7 we present our conclusions.

2. ANALYTIC MODELS

To create an analytic model that can determine if the SASI is an advective-acoustic or purely acoustic model, we start with a one-dimensional model. We begin with the time-dependent fluid equations for an ideal gas, where the fluid variables are u = velocity, p = pressure, and ρ = density. Looking for a steady-state, radially symmetric solution, the fluid equations become

$$\frac{u}{r^2}\frac{d}{dr}\left(r^2\frac{d\rho}{dr}\right) = 0 \tag{1}$$

$$\frac{\rho}{r^2}\frac{d}{dr}\left(r^2\frac{du^2}{dr}\right) + \frac{1}{r^2}\frac{d}{dr}\left(r^2\frac{dp}{dr}\right) = -\frac{GM}{r^2} \tag{2}$$

$$\frac{u}{r^2}\frac{d}{dr}\left(r^2\frac{d\rho}{dr}\right) - \frac{\gamma p u}{\rho r^2}\frac{d}{dr}\left(r^2\frac{d\rho}{dr}\right) = (1-\gamma)\mathcal{L} \tag{3}$$

where $\mathcal{L}$ is the cooling function defined by $\mathcal{L} = A\rho^{\beta-\alpha}p^{\alpha}$.

We assume that the velocity of the accreting gas is at free-fall once it hits the shock radius. To

model the fluid variables at the shock radius r_s, we use Rankine-Hugoniot shock conditions:

$$u_s = -\frac{\gamma-1}{\gamma+1}\sqrt{\frac{2GM}{r_s}}\,, \tag{4}$$

$$p_s = \frac{2\dot{M}}{4\pi(\gamma+1)}\sqrt{\frac{2GM}{r_s^5}}\,, \tag{5}$$

$$\rho_s = \frac{\dot{M}(\gamma+1)}{4\pi(\gamma-1)}\sqrt{\frac{2GM}{r_s^3}} \tag{6}$$

We normalize the problem so that GM=1/2, $\dot{M}$ = 4π, and $r_s = 1$.

We consider two different models, one radiative with a hard inner boundary and one adiabatic with a leaky inner boundary. The former is perhaps more directly related to the core-collapse scenario, but introduces some ambiguity into the location of the coupling radius for the advective-acoustic model. The adiabatic model is more ad-hoc in that it requires an inner boundary with a fixed rate of mass flux in order to create a steady state, but it has the advantage that there are no features in the flow to create a coupling radius other than the inner boundary itself.

For the radiative model, we follow Houck & Chevalier (1992) and integrate the solutions to equations 2 & 3 from the shock radius, r_s=1, down until u=0, where the accreting mass settles on the PNS, r_*. For these solutions, we set $\alpha = 3/2$ and $\beta = 5/2$, following Foglizzo et al. (2007). We chose the cooling coefficient to produce a PNS radius r_* of .3.

For the adiabatic model, following Blondin et al. (2003) and ignore the effect of neutrino cooling. We also assume that the gas is isentropic such that p/ρ^γ is constant. From equation 3, we obtain the bernoulli equation to describe the post-shock flow

$$\frac{1}{2}u^2 + \frac{\gamma}{\gamma-1}\frac{p}{\rho} - \frac{GM}{r} = 0 \tag{7}$$

Using our normalized parameters, we can rewrite the Bernoulli equation to be of the form

$$ru^2 + \alpha r^{3-2\gamma}u^{1-\gamma} - 1 = 0 \tag{8}$$

where

$$\alpha = \frac{4\gamma}{(\gamma+1)(\gamma-1)}\left(\frac{\gamma-1}{\gamma+1}\right)^\gamma \tag{9}$$

We again chose r_* to be .3.

We can use these models to illustrate the dependence of the acoustic and advective-acoustic periods on the ratio of specific heats of the gas. The acoustic mechanism is modeled as a sound wave propagating around the PNS at a fixed radius inside of the accretion. The dominant l=1 mode of the SASI is thus a wave that bounces back and forth at the poles. Thus, the time for one oscillation can be calculated by

$$\tau_1 = \frac{2\pi r_a}{c_s}, \tag{10}$$

where c_s is the sound speed at the effective propagation radius r_a.

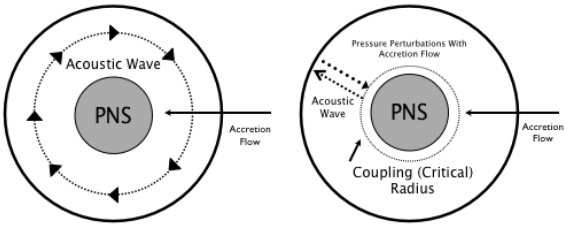

Fig. 1.— Schematic diagram showing the acoustic mechanism (*left*) and the advective-acoustic mechanism (*right*). The dark outer circle is the shock radius.

The period of the advective-acoustic mechanism will include the time for a perturbation to advect radially inward with the shocked accretion flow plus the travel time for the pressure wave that propagates against the accretion flow at the local speed $c_s - u$. Thus, the time for one advective-acoustic cycle is

$$\tau_2 = \int_{r_s}^{r_c}\frac{dr}{u} + \int_{r_c}^{r_s}\frac{dr}{c_s - u} \tag{11}$$

For the radiative model, to keep r_* set at .3, we calculate the fluid variables for various γ, and change the cooling coefficient to maintain r_*=.3. The cooling coefficient thus becomes a function of γ:

$$A(\gamma) = 5.13\times10^{-4}\,\gamma^{55.596} \tag{12}$$

Both of these models involve an adjustable parameter. For the adiabatic model we have an effec-

tive radius of propagation, and for the advective-acoustic model we have an effective coupling radius. Our approach is to choose these values in order to match the models with the observed oscillation period of the SASI for $\gamma = 4/3$, and keep them fixed at those values as γ is changed. Keeping r_*=.3, we set $r_a \approx .8$ and $r_c \approx .32$. The resulting dependence of the oscillation period of these models on γ is shown in Figure X. By design the two models are matched at $\gamma = 4/3$, but as γ decreases the timescale for the advective-acoustic model rapidly increases. By studying the SASI at smaller values of γ we can potentially distinguish between these two models.

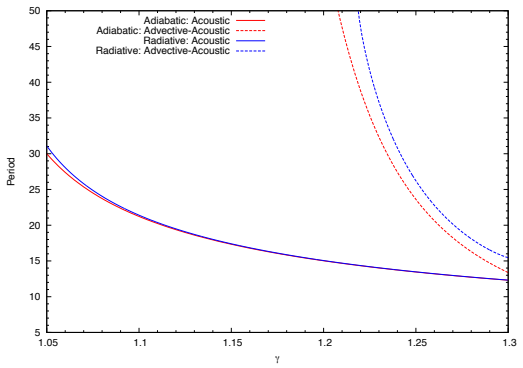

Fig. 2.— This plot shows the time for each mechanism as a function of γ. This plot is for the radiative case. Note that for γ=4/3, the time for each cycle is the same. A slight decrease in γ shows that the advective-acoustic cycle takes longer than the acoustic cycle.

3. SASI IN TWO DIMENSIONS

Two dimensional simulations were used in analyzing each mechanism in order to determine what actually drives the SASI. Using the same 400 zones with a leaky inner boundary at r_*=.3 and a fixed inflow at the outer boundary. We add in the polar angle to create a spherical grid. We cover the polar angles from 0 to π over 200 zones, assuming axisymmetry about the polar axis.

We ran simulations for various values of γ, from 4/3 to 1.3. We confined our simulations to γ values to between 1.3 and 4/3, since it is unreasonable to think of a supernova with γ much lower.

VH-1 uses a piecewise parabolic method (Colella & Woodward 1984), where shock transitions are confined to two zones. This method creates numerical noise in two dimensions with the pressure and density. In order to quiet this down, we use the same "wiggling" described by Colella & Woodward (1984).

In order to excite the growth of the l=1 mode, we add in a small radial density perturbation at the shock. Since we are only interested in the linear growth of the SASI, we stop the simulation once the perturbed shock reach the outer boundary.

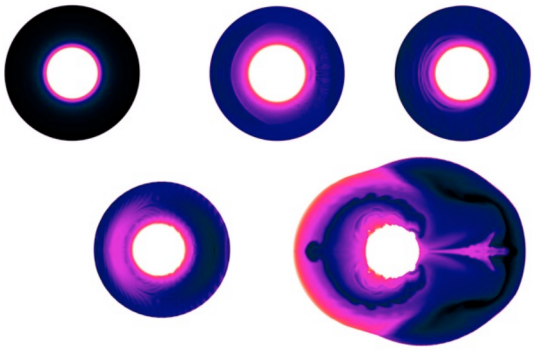

Fig. 6.— This shows the time evolution of the SASI. The SASI progresses from left to right, beginning with a steady shock. The second image clearly shows the l=1 mode. As time progresses, turbulence grows behind the shock to lead the SASI out of the linear phase and into the nonlinear phase, shown in the bottom right image. This nonlinear phase leads drives the supernova from there on.

Figure 6 illustrates the growth of the SASI in two dimensions with respect to the entropy. The shock begins as stable and spherically symmetric. From that point, we can visually see the growth of the l=1 mode, where we see turbulence that is bouncing between the poles. This entropy interacts with the shock, which causes the spherical

symmetry to be broken and begins the non-linear phase of the SASI. This is shown as the last image, where it has clearly become spherically asymmetric. The growth of this nonlinear phase is what leads to the supernova.

During the simulation, we calculate the linear momentum in order to track the linear growth of the SASI. If we plot the linear momentum vs. time, we can create a fit for the growth of the SASI. Figure 6 shows the growth of the SASI with a fit. In order to fit the data, we track the linear momentum, $\mathcal{P}$, as a function of time of the form

$$\mathcal{P}(t) = A_0 e^{\omega_r t} \cos(\omega_i t + \delta)\,, \qquad (13)$$

where ω_r is the growth rate and ω_i is the oscillation frequency. We plot linear momentum and the fit as time progress in figure 7.

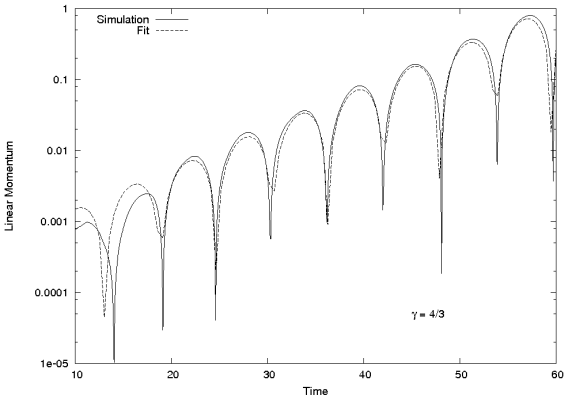

Fig. 7.— This figure shows the linear momentum of the SASI. A fit (*dashed*) of the SASI (*solid*) is shown during the linear phase. From this plot, we can obtain the growth rate ω_r and the oscillation frequency ω_i

Using a linear least squares algorithm, we find the error in ω_i after fixing the amplitude, phase shift, and ω_r. Repeating for various γ, we can calculate the period and error in period and plot the period as a function of γ. This allows us to compare the advective-acoustic and the acoustic description of the SASI versus the simulations, to see which description is more accurate. Figure 8 shows the simulations against the analytic models put forth in §2. We see that the simulations lie directly in the middle of the two models.

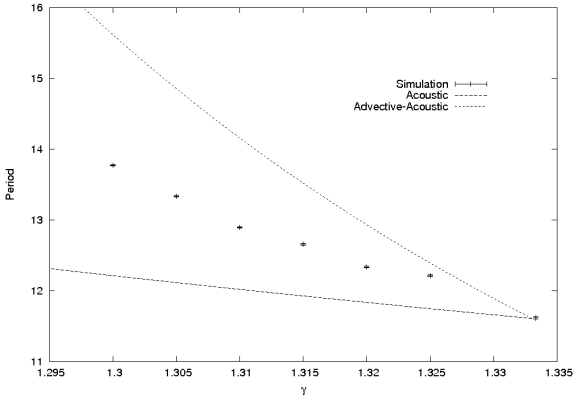

Fig. 8.— This shows that as γ is slightly lowered from 4/3, both of the current explanations of the SASI fail to match the simulations. This indicates that neither description are complete descriptions of the SASI

3.1. Adiabatic Model

We note that for the description of the advective-acoustic mechanism, if there is no cooling function and we just apply a leaky inner boundary, i.e, the adiabatic version, the coupling radius for the advective-acoustic is fixed at the inner boundary. We have chosen the inner boundary for the simulations to be r_*=.3, so the coupling radius in the adiabatic model is fixed at .3, for any γ value. Since we know that the period for the acoustic mechanism and the advective-acoustic mechanism are equivalent at γ=4/3, we chose the parameter for the analytic models to fit the simulations at 4/3. Since the coupling radius is fixed, there is no way to shift the advective-acoustic curve down toward the simulation data by changing the inner radius. We can also not shift the acoustic mechanism up toward the simulation data because the period is dependent of the radius of the acoustic wave, which we fixed to match at γ=4/3. For the less physical adiabatic model, we show that neither mechanism offers a strong enough description to match the data if γ we slightly lower than 4/3.

3.2. Radiative Model

We approach the radiative analysis similar to the adiabatic. We span 396 zones for the radius exactly like the one-dimensional case. We span 180 degrees with 180 zones. Instead of imposing a leaky boundary condition, we instead add in a cooling function to model the neutrino cooling. We use the parametrized cooling function

$$\mathcal{L} = \rho^{\beta-\alpha} p^{\alpha} \tag{14}$$

Following Foglizzo et al. (2007), we choose α=3/2 and β=5/2.
We track the linear momentum exactly like in §4. We use the same functional form for the fit and also perform linear least squares to find the error in the oscillation frequency. We relate this to the period of oscillation for the SASI and compute the error in period. For the radiative simulations, we performed simulations with $1.2575 \leq \gamma \leq 4/3$. For each γ value, we plot the periods as a function of γ and compare it with our analytic analysis. This is shown in figure 9.

Figure 9 shows us that including neutrino cooling in our simulation also results in periods that lie directly between the current theories. For the radiative case however, the coupling radius is not confined to the inner boundary. Thus, the coupling radius can change as γ is changed. In order to address this point, we analyze the flow properties to see if there is anything about the coupling radius that would require it to be a specific value.The approach we establish in §2 calculates the oscillation period for each mechanism. Because previous research has shown that both the acoustic and advective-acoustic description will oscillate at comparable time-scales for γ=4/3, we use the results from the simulations and match up the period curves at γ=4/3. In order to do this, we had to choose an acoustic radius, r_a, and a coupling radius, r_c, so that the curves matched for γ=4/3. This coupling radius is characteristic of the advective-acoustic theory. Thus, if the advective-acoustic theory was the correct description of the SASI, this r_c should be unique. Keeping the PNS radius r_*=.3, the coupling radius that agrees with our results is r_c=.3255. We analyze this radius, in order to see if there is any obvious property of the flow that could lead to this coupling. Figure 10 shows various properties of the flow as a function of radius, indicating the required coupling radius.

As shown in the graph, there is nothing unique about this critical radius. It corresponds to no extrema in any of the flow properties. We should expect that this coupling radius, where the advection turns to the acoustic wave to travel back out to the shock, would correspond to some property of the flow. This is not the case.

We would also like to note that the flow profile does not change drastically with variable γ. If we look at one feature of the flow, entropy in this case, we see that as we decrease γ we do not find much change. Figure 11 shows this for $\gamma = 1.31$, 1.29, & 1.27

A drastic change in the flow profile may indicate a change in the coupling radius. We see from Figure 10 that there is nothing in the flow profile for γ=4/3 that would indicate a specific radius. Now that we see no drastic change in the entropy profile for varying γ, we have no reason to think that there is any more evidence for a specific coupling radius for any γ. Thus, we are free to chose a coupling radius in order to match our simulations at γ=4/3. From this, figure 9 clearly shows that the period for the SASI lies directly between the proposed mechanisms.

We further show that neither description are adequate in describing the SASI by analyzing the period as a function of coupling radius for γ=4/3. This is shown in Figure 12, which indicates that for the acoustic mechanism, the period of oscillation is constant because it does not depend on r_*. As for the advective-acoustic mechanism, the calculated period is dependent on r_*. We know that the period for the advective-acoustic description equals the acoustic description for γ =4/3. This occurs when the PNS radius is approximately .25. Yet, neither descriptions match the simulation results at this radius. Also, we see that neither mechanism matches the simulation results for all PNS radii, which we would expect from an adequate model. From this, the radiative period vs. γ plot and the adiabatic period vs. γ plot, we conclude that neither mechanism can be used to adequately describe the SASI.

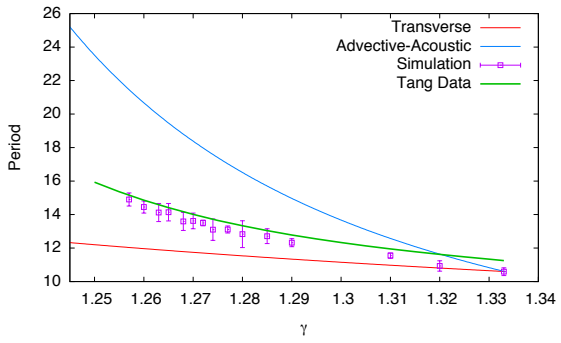

Fig. 9.— Radiative plot of period vs. γ. This shows that both the advective-acoustic mechanism and the acoustic mechanism do not fall within the error of our simulations, indicating that the proposed descriptions are inadequate for lower γ.

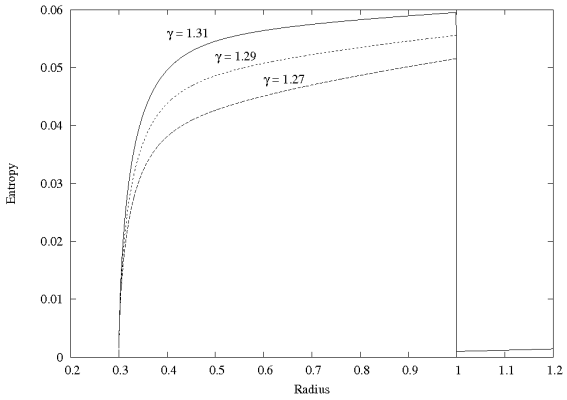

Fig. 11.— Entropy profiles for various γ

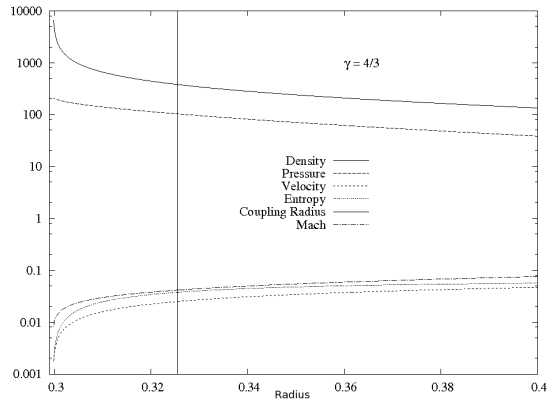

Fig. 10.— Plot of flow properties for γ=4/3 with the coupling radius of .3255

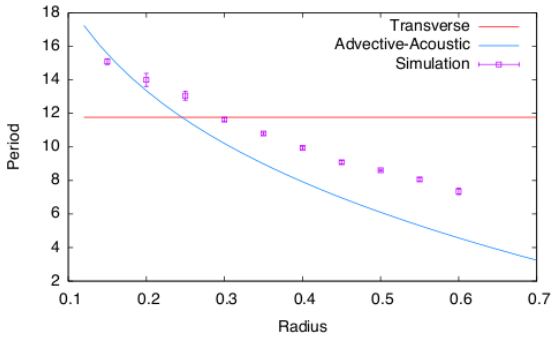

Fig. 12.— This shows the dependence of each description on the coupling radius. The acoustic mechanism has no r_* dependence, whereas the advective-acoustic description is highly dependent on r_*

4. CONCLUSION

The model presented in this paper is a simple model that analyzes both the advective-acoustic an acoustic description and their ability to describe the SASI . The previous problem has been that when analyzing supernova, the acoustic and advective-acoustic description go through one oscillation at comparable times. Thus, simulations and analytic models have not necessarily been able to distinguish between the two. Evidence for both theories have been presented prior to this paper. Blondin et al. (2006) provides simulation evidence supporting the acoustic description, whereas Foglizzo et al. (2007) provide a thorough description of the advective-acoustic theory. Analysis of both of these shows that when γ=4/3, it is hard to establish which theory is correct because of the time similarity. We approach this problem trying to find a regime where these time scales become disparate.

We note that a regime when the periods become disparate occurs if the adiabatic index is lowered. This is because the post-shock sound speed stays fairly constant as opposed to the increasing time of advection, due to the changed compressibility of the gas. Thus, our approach was to use the same initial conditions and boundary conditions, except changing γ accordingly, to create simulations for each γ. Doing this, we stay true to the dynamics of the core-collapse supernova. Tracking the linear momentum was a simple way to track the growth of the SASI, where we can extract both a growth rate and oscillation frequency. This oscillation frequency can be related to the period for each oscillation during the linear growth phase, which corresponds to the period of either a sound wave traveling around the shock (acoustic description), or perturbations falling inward and coupling to travel back out (advective-acoustic dsecription). For both the purely adiabatic simulations and the radiative simulations we find that the SASI does not favor either model.

We note that our model observes the SASI in a regime where the material inside the shock is modeled as material different from a γ=4/3 gas, as described by Janka (2001). Because we know that the advective-acoustic mechanism and the acoustic mechanism oscillate at the same period for γ=4/3, we know that we can choose a coupling radius and acoustic radius to match our simulation data at that adiabatic index. We are free to do this because there is no obvious property of the flow that would lead to coupling, the flow profile does not change much with γ. There is nothing in the difference of flow profiles to suggest that the coupling should change. Although both descriptions can be made to match at 4/3, our results show that lowering γ forces the descriptive power of each to break down. We further showed that if we change the PNS radius, both descriptions do not match the simulations, indicating that even for γ=4/3, both the advective-acoustic model and the acoustic model have limited descriptive power.

We do acknowledge that for core-collapse supernova, the material inside the shock is modeled as a γ=4/3 gas. Our simulations are unphysical in that sense, but if we rely on either mechanism to model the SASI, it should hold for any γ value. So although they were unphysical, our simulations for various γ values indicate that each are weak descriptions. We conclude that neither the acoustic or advective-acoustic mechanism can be used to describe the SASI. During the linear phase, the period for the SASI is highly dependent on the PNS radius as well as the adiabatic index. For the advective-acoustic description, the period does rely on the PNS radius, but does not model it accurately. It also fails in the having the same γ dependence, because it has a longer period for lower γ than the SASI. The acoustic mechanism fails in that it has no PNS radius dependence, and results in a shorter period than the SASI for lower γ. We propose a new model in which there is some interplay between the two mechanisms so that we can fully model the SASI during the linear phase of growth. More research will be done on this theory so we can fully understand the SASI and supernovae in general.

REFERENCES

Blondin, J. M., & Mezzacappa, A. 2006, ApJ, 642, 401

Blondin, J. M., & Shaw, S. 2007, ApJ, 656, 366

Blondin, J. M., Mezzacappa, A., & DeMarino, C. 2003, ApJ, 584, 971

Colella, P., & Woodward, P. R. 1984, J. Comput. Phys., 54, 174

Foglizzo, T., Galletti, P., Scheck, L., & Janka, H.-Th. 2007, ApJ, 654, 1006

Houck, J. C., & Chevalier, R. A. 1992, ApJ, 395, 592

Janka, H.-T. 2001, A&A, 368, 527

Mezzacappa, A., Calder, A. C., Bruenn, S. W., Blondin, J. M., Guidry, M. W., Strayer, M. R., & Umar, A. S. 2001, ApJ, 495, 911

Ohnishi, N., Kotake, K., & Yamada, S. 2006, ApJ, 641, 1018

This 2-column preprint was prepared with the AAS LaTeX macros v5.2.